

PROJECT CODE

EA006

Abstract

Earthquake location is extensively useful, for both theoretical and applicational purposes. This report explores a new direct search algorithm that matches the earthquake location to the minimum of square of misfit between the observed travel time and pre-determined travel time with respect to origin time. Eikonal equation solves for the generation of travel times in inhomogeneous seismic velocity models under a discretised sampling space model. A mathematical model is used to simulate a real-life inhomogeneous seismic velocity model to test this algorithm; followed by numerical tests to study the effects of (i) different grid sizes, (ii) random errors on arrival times, (iii) cumulative effects of both random errors and different grid sizes on the accuracy of the earthquake location. Factors affecting the accuracy and precision of results include choice of objective function, assumptions in the Eikonal-based model, grid resolution, and random errors. While choice of objective function and the assumptions in Eikonal-based models could affect the accuracy and precision in locating earthquakes, more attention should be paid to the effects of grid resolution due to computational limitations. The effects of random errors on accuracy of earthquake location are significant, implying the need for further studies on the mentioned effect under the statistical point of view.

EIKONAL EQUATION-BASED GRID SEARCH METHOD FOR PRECISE EARTHQUAKE LOCATION

Nguyen My Bin An, Tran Phuoc My

INTRODUCTION

In general, there is much demand for accurate & precise location of earthquakes for seismic studies, research into the geology into a certain region (e.g [1]), and real-life planning and developments that take into account the nature of earthquakes and their locations (e.g [2]). This report explores a new algorithm to search for precise earthquake location. To test the algorithm under different real-life situations, we use synthetic data that closely mimics real-life set-ups. The synthetic data is inspired by well-studied seismic velocity models (e.g [4]).

High-velocity Primary waves (*P-waves*) [3] are useful as seismic data [3, 5, 6]. Yet its velocity is not constant due to the inherent nature of the region's geology [3]. The inhomogeneous nature of seismic velocity poses a challenge to calculate the travel time, suggesting the need of appropriate model to be used. Thus, seismic travel times must be generated computationally with the help of a model that could address the problem of inhomogeneity.

Assuming the earthquake is located at a given point in a grid space, we can calculate the difference between the *arrival time* and *receiver time* (with the origin time considered) (Annex A). An *objective function* of all the time differences for all receivers is introduced. Finding the global minimum of this objective function gives an approximation of the earthquake's true location.

LITERATURE REVIEW

1. Generating Seismic Velocity Model from Real-life Seismic Data

A grounded and realistic velocity model is crucially foundational in accurate earthquake locations. As such, we utilise the well-studied model of the seismic structure in Transverse Ranges, California, as the basis for our velocity model [4] & other numerical tests. The visualization of this basis seismic velocity model is named **Model2D** (Annex B).

2. Solving Eikonal equations in Inhomogeneous Velocity model

Solving Eikonal equation for travel times in an inhomogeneous medium:

$$\nabla u(x, z) \cdot \nabla u(x, z) = \frac{1}{v(x, z)^2}, \quad x, z \in R$$

Where:

$v(x, z)$: velocity

$u(x, z)$: travel time from a receiver to (x, z)

with boundary condition:

$$u(x_k, z_k) = 0, \quad k \in \{1, 2, 3, \dots, 9\}.$$

(x_k, z_k) denotes coordinates of receiver k . This process can be expedited by the Fast Sweeping Method

(FSM) [7] (Annex C) . From this equation, we also define the grid size as h^1 .

RESULTS

1. Generating Timetables & Arrival Times at each Receiver

In reality, seismic data is often obtained in regions where the geology experiences buckle-folds in its strata [21], demonstrated by **Model2D_true** (Fig 1).

Note that the seismic velocity model in real life in different places differs from one another due to this nature of geology (Annex D), hence, the seismic velocity obtained in **Model2D** (Annex B) is not generalized enough to cater to various real-life

situations where geology plays an important role in deciding the actual seismic velocity model at that particular region.

However, the generation of such real-life seismic data (any form of **Model2D_true**) can be executed to simulate that real-life situation with minimal inaccuracy using period functions, such as sine. In our case, a **Model2D_true** is taken and simulated from **Model2D** by the following function:

$$v_{true} = v(x, z) \times (1 + 0.1 \sin\left(\frac{\pi x}{25}\right) \sin\left(\frac{\pi}{4} \times (\sqrt{25 - 8z} - 5)\right)), \quad z < 0$$

where: $v(x, z)$ is P-wave velocity at coordinates (x, z) in the velocity model **Model2D**, $v_{true}(x, z)$ is that of **Model2D_true**.

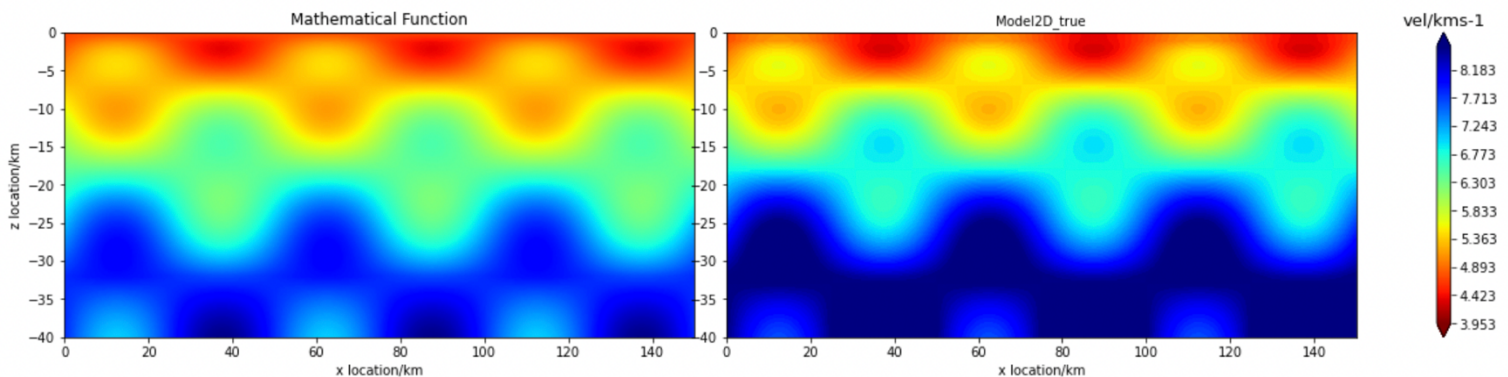


Fig 1. Simulating seismic velocity model (**Model2D_true**) with real life mathematical function

Re-modelling the real velocity model **Model2D_true** is important in generating both *timetables* and *arrival times* from the earthquake to the Receiver, which is done by solving Eikonal equation, given the distance calculated by the coordinates. The timetable was modelled to a grid with interval of 0.2 km along the x and z location (hence, grid size $G = 0.2$).

The model predicts the desired earthquake to be located at nodes of the grid. Isochrone maps of 1s interval at each Receiver are drawn to highlight the possible locations – from where earthquake start will reach the respective station with approximately the same amount of time recorded at the stations to the timetables (Annex E).

¹ In this section, h is used to denote grid size. However, from section 1 of Results onwards, G is used instead to denote grid size.

Predictably, the earthquake shall locate nearest to 9th Receiver and farthest to 1st Receiver. Similarly, the arrival times from earthquake to receivers are also calculated, known as ‘time to get first P wave’ in the below data frame.

ID	x location	z location	origin time	time to get first P wave/s
0	1.0	10.0	0.0	20.4408
1	2.0	20.0	0.0	19.0140
2	3.0	30.0	0.0	17.8133
3	4.0	40.0	0.0	16.7090
4	5.0	50.0	0.0	15.1751
5	6.0	60.0	0.0	13.4421
6	7.0	70.0	0.0	11.9708
7	8.0	80.0	0.0	10.6728
8	9.0	90.0	0.0	8.8627

Fig 2. Generating Arrival Times from the earthquake to each station based on Eikonal equation

2. Earthquake Location: Objective Function

a. Objective Function

If we assume the earthquake to locate at grid point (i, j) , the arrival time from the earthquake to all stations is then equal to the time a P-wave from that grid point (i, j) travels to the corresponding stations. As earthquake originates at a non-zero origin time τ , the real time of travel of earthquake is $T_{obs} - \tau$. The earthquake location therefore minimises the following objective function (Annex F):

$$\min \sum_{k=1}^9 [T_{i,j}^k - (T_{obs} - \tau)]^2$$

where: k denotes the index of Receiver

T_{obs} : time for earthquake to reach a Receiver

$T_{i,j}$: time travelled from the grid point (i, j) to Receiver

τ : origin time when earthquake starts

b. Calculating τ

From the objective function, the time origin τ of the earthquake is unknown despite its significance in locating the earthquake. Since the earthquake location achieves the minimum of objective function, differentiating the Objective Equation with respect to τ and equate it to 0 to solve for τ yields the result of:

$$\tau = 3.46 \times 10^{-2} s$$

3. Grid-search: Relocate Earthquake

Synthesizing the real-life seismic data also yields the modelled earthquake location at grid size $G = 0.2$ at $(x, z) = (135.80, -15.00)$. With this given earthquake as previously known, the accuracy of our algorithm is investigated by comparing the assumed-known earthquake to the located one.

With the known value of the modelled earthquake location at $(x, z) = (135.80, -15.00)$, 9 timetable maps for this location are plotted to show the time P wave from each grid point takes to travel to 9 receiver (Annex E).

Value of objective function between T_{obs} and $T_{i,j}$ at 188 501 points on the 751 x 251 grid for each Receiver is calculated and presented in a DataFrame – where 9 time differences at each point is summed up and programming code is used to traverse the list to find the position where minimum sum occurs.

	Cal1	Cal2	Cal3	Cal4	Cal5	Cal6	Cal7	Cal8	Cal9	sum
0	13.320495	11.406566	9.474912	7.461921	4.896949	2.051279	0.586255	3.085527	6.119960	58.403864
1	13.345218	11.429032	9.494480	7.478531	4.910869	2.062905	0.576510	3.077293	6.112927	58.487766
2	13.369931	11.451468	9.513998	7.495074	4.924711	2.074449	0.566849	3.069139	6.105970	58.571587
3	13.394635	11.473874	9.533464	7.511549	4.938474	2.085909	0.557270	3.061065	6.099088	58.655328
4	13.419329	11.496250	9.552877	7.527954	4.952157	2.097285	0.547776	3.053073	6.092284	58.738985
...
188496	4.622130	4.763241	4.649114	4.370683	4.442442	4.627821	4.460293	4.023408	3.999457	39.958589
188497	4.662791	4.803769	4.688935	4.409426	4.479912	4.663793	4.494502	4.055556	4.029227	40.287910
188498	4.703725	4.844567	4.729023	4.448439	4.517658	4.700046	4.528999	4.088002	4.059307	40.619767
188499	4.744936	4.885638	4.769381	4.487726	4.555682	4.736582	4.563787	4.120748	4.089701	40.954181
188500	4.786424	4.926984	4.810009	4.527288	4.593986	4.773405	4.598869	4.153797	4.120410	41.291173

188501 rows × 10 columns

Fig 3. Calculation of Objective Function at grid points for 9 stations (Cal1 represents the values of objective function of all grid points at Receiver 1)

Traversing the list of grid points for its position, the 170508-index point is found to be at position **(135.80, -15.00)**.

Cal1	Cal2	Cal3	Cal4	Cal5	Cal6	Cal7	Cal8	Cal9	sum	
170579	0.054144	0.089455	0.007434	0.249611	0.122774	0.142425	0.087414	0.193567	0.003216	0.950039
170580	0.033543	0.109960	0.012208	0.231684	0.106895	0.155878	0.097972	0.186496	0.000412	0.935049

```
1 idxmin = int(S[S["sum"]==S.min()]['sum'].index.values)
2 # idxmax = int(S[S["sum"]==S.max()]['sum'].index.values)
3 print(idxmin)
```

170580

```
1 dfmodel2D[(idxmin-1):(idxmin+1)]
```

x z vel/ms-1

170580	135.800002	-15.0	6.10
170581	135.800002	-14.8	6.08

Fig 4. Finding location of earthquake by traversing the list for minimum of sum of time difference

At this position, the objective function achieves minimum and close to 0 (Annex F).

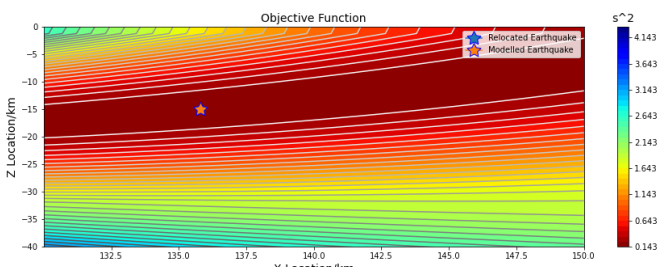


Fig 5. Minimum of Objective Function at earthquake relocation position

4. Accuracy of Grid Search Method

a. Different Grid – size (G)

Applying the algorithm on 4 different grid sizes to study the effects of grid size on the accuracy of the algorithm. Generally, greater grid size results in the greater deviation of earthquake location.

G	Modelled	Relocated	Error
	Earthquake	earthquake	
0.05	(135.40, -15.55)	(135.95,-15.35)	(0.50, 0.20)
0.10	(135.70, -15.30)	(135.90, -15.30)	(0.20, 0.00)
0.20	(135.80, -15.00)	(135.80, -15.00)	(0.00, 0.00)
0.25	(136.25, -14.75)	(135.75, -14.75)	(0.50, 0.00)
0.50	(136.00, -14.50)	(135.50, -14.5)	(0.50, 0.00)

Table 1. Comparison of Earthquake Locations under different uses of grid sizes

b. Influence of Random Errors

Uncertainties in earthquake locations are caused by the measurement of errors of seismic arrival times [16, 15], studying which further informs the accuracy of our algorithm and its applicability and validity in real life. 100 sets of random errors ($N=100$) within $\pm 0.2\text{s}$ [12] are generated at each station to simulate the situations in real life. 100 earthquake locations are found and observed to mainly cluster within a specific region despite few outliers observed in all 5 studied grid size models (Annex G).

Error of locating earthquake is measured as the distance between the modelled earthquake and the located earthquake. Multivariate linear regression model thus predicts the radius of region in which the located earthquake will lie in under the different sets of random errors. Summary statistics of those regression models using measurement errors of suggest that the

prediction of location error from such regression model is large.

	G = 0.05	G = 0.10	G = 0.20	G = 0.25	G = 0.50
R²	0.080	0.079	0.091	0.142	0.205
RMSE	0.9549	0.8705	1.0788	0.9344	0.9508
MSE	0.9119	0.7577	1.1638	0.8731	0.9040

Table 2. Summary statistics of regression models to predict the deviation of earthquake location

The density distribution of earthquakes is demonstrated by the overlap of circles which demonstrate the predicted areas within which earthquake will lie (Annex H). With a grid size of 0.2, confidence level of 95% is made that the earthquake will lie within a 2.14km radius from the real modelled earthquake regardless of the effect of random errors in any range.

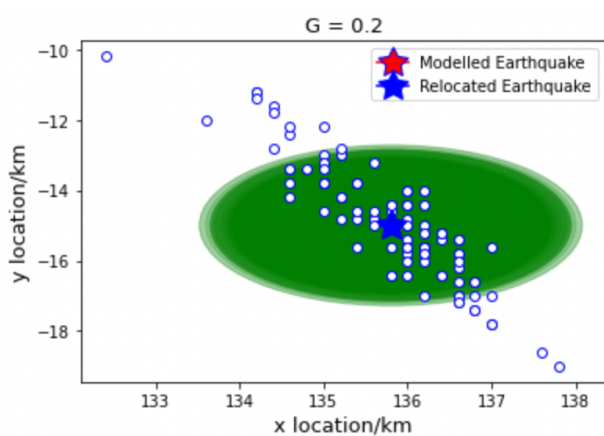


Fig 6. Example of density distribution of earthquake location under the influence of random error of any range

The test expands to compare the confidence region of earthquake location in the case where random error ranges from $\pm 0.2\text{s}$ to that under the influence of any random errors. Further details for other grid sizes are summarized in table below (Table 5).

Confidence Radius	G = 0.05 (km)	G = 0.10	G = 0.20	G = 0.25	G = 0.50
General	2.07	1.86	2.14	2.33	2.39
Sample	2.50	2.36	2.14	2.52	2.57

Table 3. Comparison of confidence radius (of 95% confidence level) of density distribution of earthquake location under the effect of random error in general situation (General) and under the effect of random error in sample data (range of 0.2s)

In grid size G = 0.1, we are confident to say that 95% of chances the earthquake found by the algorithm under the random errors of $\pm 0.2\text{s}$ will locate within a radius of 2.36km from the real earthquake; whereas we are confident to say that 95% of chances the earthquake under any random errors will locate within a radius of 1.86km.

DISCUSSION

1. Eikonal Equations to solve Timetables and Arrival Times

The Eikonal equation is most applicable in simulations of wave propagations, where the wave functions are approximated via the Wentzel–Kramers–Brillouin (WKB) approximation [13]. More specifically, the WKB approximation is often used in semiclassical calculations which recast wave functions as exponential functions in a semiclassical expansion [14]. However, the mathematical model that approximated the velocity model in real life utilised mostly periodic functions, which deviates from the context in which the WKB approximations hold, and similarly for the assumptions that the Eikonal equation operate best under. This may result in some computational results, such as the arrival times, deviating from expectations.

Additionally, arrival times gathered from real-life seismic stations will always have a certain degree of uncertainty attributed to them, either through the extrinsic random errors [12] or through the intrinsic nature of the geology in the region that the seismic waves propagate through [18]. This also means that attempts at simulating such geological conditions in a velocity model and using Eikonal-based algorithms to compute arrival times will also have intrinsic biases due to the model chosen. Hence, the periodic nature of the variations in our mathematically simulated velocity model could have been a common bias throughout the arrival times generated.

Computationally speaking, the Eikonal equation has the FSM [7] which rapidly expedites the process of approximating solutions for it. Much work in this report lies in extracting travel times in an inhomogeneous system, which was done almost entirely via algorithms. As such, a method that expedites this process is helpful in reducing computational times and enabling numerical tests with finer precision, which helps to reduce inaccuracies.

The Eikonal equation is also more applicable for our purposes than other similar equations working in an inhomogeneous model. One possible alternative could have been the Hamilton–Jacobi–Bellman (HJB) equation that gives the condition for optimality with respect to an objective function [15]. However, the HJB equations admits classical solutions only for sufficiently smooth objective functions – a property not universally guaranteed [16], especially after discretisation of the velocity model as in our work.

2. Objective function

The choice of a quadratic function was meant for two reasons. Firstly, as the objective function must be differentiated and equate to 0 to find the stationary points that indicate the minimum value of the objective function and thus finding the origin times, the function is preferred to be of a form that is easily differentiable – which quadratic was highly suitable. Additionally, the use of an exponent greater than 1 in summing the time differences in the objective function seeks to place a greater-than-proportionate significance on larger differences within the function, thereby ensuring that the overall minimum would include very minor deviations across all terms. This is especially important in our high-precision task that wishes to minimise large deviations from expected results, but is more tolerant towards smaller deviations that are potentially due to unavoidable uncertainties in measurements [12].

3. Accuracy of Earthquake Location Model under different scenarios

3.1 Different Grid Sizes

The choice of grid-size determines the significance of error in earthquake locations. Smaller grid size causes the spatial distance (between grid points and stations) and objective function to be relatively closer to each other. With insignificant differences between spatial distance, deviation of minimal sum of objective function with different grid sizes is small, leading to small error of earthquake location. However, notably, with very small grid size of $G = 0.05$, error of earthquake location is much more significantly larger than the rest. The deviation of earthquake location in very small grid size may arise due to extreme proximity of grid points. Under computational

limitation in handling numbers with great precision, traversing the grid for minimum of objective function in this case may not be optimal and precise to match the precision of minimal proximation of objective function at grid points.

3.2 Under influence of random errors

In earthquake monitoring, system timing is key to locating earthquake. Any errors in timings will cause a deviation of earthquake location from the true position. Yet, random error is inevitable. It can come from various sources [17, 18, 20]. These random errors cause the errors in calculating arrival times, leading to a relative location scatter around the true earthquake location. Hence, random errors determine the precision of location of earthquake. In the problem of earthquake location, random errors are treated from a purely statistical point [17]. Proper handling of modelling errors of calculated travel times is difficult in earthquake location, mostly because the error is unknown [17].

With a distraction of earthquake location arisen from random error, further study of the extent to which earthquake location deviates from the actual one under these influences is made so that the exact location can be found in consideration of the possible deviation. The prediction of spatial radius in which earthquake may lie using multivariate linear regression assumes the normal distribution of errors which in real life may not hold. Moreover, summary statistics of those regression models with large measurement errors of RME, SME, MAPE implies the unsuitability of the

regression models in predicting the accuracy of earthquake location under effects of random errors. However, those models are largely effective in analyzing the confidence region of probabilistic density distribution of earthquake. Overall, the confidence region of earthquake location is smaller than that of the situation where the random error is to be within a specified range. Moreover, the confidence region of earthquake location is smaller, implying the better accuracy of earthquake search method, for smaller grid size. The explanation of computational limitations in handling too-proximate numbers still hold true for extremely small grid such as $G = 0.05$, causing the confidence region of earthquake location to be higher than expected.

CONCLUSION

The algorithm to find the absolute earthquake location provides a direct search with high accuracy. As a non-linear method, it is advantageous in obtaining a complete solution with uncertainties. The choice of grid sizes in sampling of model spaces plays a role in determining the accuracy of the model. Random errors affecting the measurement of arrival times pose a concern of accuracy to our models due to the high level of uncertainties in the distribution of earthquake arises. The model thus transforms the solution from absolute location to relative location in this case. If time permits, further work could have been done to study the extent of impact of random errors on the earthquake location. Regression models are applied in this case yet are not suitable due to high errors in prediction of the deviation of earthquake location.

BIBLIOGRAPHY

1. Martínez-Loriente, S., Gràcia, E., Bartolome, R., Sallarès, V., Connors, C., Perea, H., Lo Iacono, C., Klaeschen, D., Terrinha, P., Dañobeitia, J. J., and Zitellini, N. (2013), Active deformation in old oceanic lithosphere and significance for earthquake hazard: Seismic imaging of the Coral Patch Ridge area and neighboring abyssal plains (SW Iberian Margin), *Geochem. Geophys. Geosyst.*, 14, 2206– 2231, doi:10.1002/ggge.20173.
2. Thomas Theunissen, Yvonne Font, Serge Lallemand, Wen-Tzong Liang, The largest instrumentally recorded earthquake in Taiwan: revised location and magnitude, and tectonic significance of the 1920 event, *Geophysical Journal International*, Volume 183, Issue 3, December 2010, Pages 1119–1133, <https://doi.org/10.1111/j.1365-246X.2010.04813.x>
3. Stein, S., & Wysession, M. (2009). An Introduction to Seismology, Earthquakes, and Earth Structure. Wiley.
4. Hadley, D., & Kanamori, H. (1977). Seismic structure of the Transverse Ranges, California. *Geological Society of America Bulletin*, 88(10)
5. Hofstetter, A., & Ataev, G. (2012). The use of P-wave spectra in the determination of earthquake source parameters in Israel.
6. Mallick, S., Craft, K. L., Meister, L. J., & Chambers, R. E. (1998). Determination of the principal directions of azimuthal anisotropy from P-wave seismic data. *Geophysics*, 63(2), 692-706.
7. Zhao, H. (2005). A fast sweeping method for Eikonal equations. *Math. Comput.*, 74, 603-627.
8. E. Rouy and A. Tourin, A viscosity solution approach to shape-from-shading, *SIAM J. Num. Anal.* 29 (1992), no. 3, 867–884. MR 93d:65019
9. M. Bardi and S. Osher, The nonconvex multi-dimensional Riemann problem for Hamilton- Jacobi equations, *SIAM Anal.* 22(2) (1991), 344–351. MR 91k:35056
10. van der Meer, D.G., van Hinsbergen, D.J.J., and Spakman, W., (2018). Atlas of the Underworld: slab remnants in the mantle, their sinking history, and a new outlook on lower mantle viscosity. *Tectonophysics* 723, p. 309-448. <https://doi.org/10.1016/j.tecto.2017.10.004>
11. Imaging Earth's Interior, Physical Geology, First University of Saskatchewan Edition, University of Saskatchewan. Retrieved from <https://openpress.usask.ca/physicalgeology/chapter/3-2-understanding-earth-through-seismology-2/>
12. Chang, C. H., Yih-Min, W., Da-Yi, C., Shin, T. C., Tai-Lin, C., & Wen-Yen, C. (2012). An examination of telemetry delay in the Central Weather Bureau Seismic Network. *TAO: Terrestrial, Atmospheric and Oceanic Sciences*, 23(3), 261.
13. Pierce, A. D. (1970). Physical interpretation of the WKB or eikonal approximation for waves and vibrations in inhomogeneous beams and plates. *The journal of the Acoustical Society of America*, 48(1B), 275-284.
14. Robinson, E. A. (1982). Migration of seismic data as WKB approximation. *Geoexploration*, 20(1-2), 7-30.
15. Yong, Jiongmin; Zhou, Xun Yu (1999). "Dynamic Programming and HJB Equations". *Stochastic Controls : Hamiltonian Systems and HJB Equations*. Springer. pp. 157–215 [p. 163]. ISBN 0-387-98723-1.
16. Bardi, Martino; Capuzzo-Dolcetta, Italo (1997). *Optimal Control and Viscosity Solutions of Hamilton–Jacobi–Bellman Equations*. Boston: Birkhäuser. ISBN 0-8176-3640-4.
17. Husen, S., and J.L. Hardebeck (2010), Earthquake location accuracy, Community Online Resource for Statistical Seismicity Analysis, doi:10.5078/corssa-55815573.
18. Gary L. Pavlis; Appraising earthquake hypocenter location errors: A complete, practical approach for single-event locations. *Bulletin of the Seismological Society of America* 1986;; 76 (6): 1699–1717. doi: <https://doi.org/10.1785/BSSA0760061699>

19. Chang, C.-H., Wu, Y.-M., Chen, D.-Y., Shin, T.-C., Chin, T.-L., & Chang, W.-Y. (2012). *An Examination of Telemetry Delay in the Central Weather Bureau Seismic Network*. *Terrestrial, Atmospheric and Oceanic Sciences*, 23(3), 261. doi:10.3319/tao.2011.11.29.01
20. Ilya Zaliapin, Yehuda Ben-Zion, Artefacts of earthquake location errors and short-term incompleteness on seismicity clusters in southern California, *Geophysical Journal International*, Volume 202, Issue 3, September 2015, Pages 1949–1968, <https://doi.org/10.1093/gji/ggv259>
21. Cosgrove, J.W., & Ameen, M.S. (1999). A comparison of the geometry, spatial organization and fracture patterns associated with forced folds, and buckle folds. Geological Society, London, Speical Publications, 169(1), 7-21

APPENDIX

Appendix	Details
Annex A	Definition List
Annex B	Seismic Velocity Model
Annex C	Solving Eikonal Equation By Fast Sweeping Method
Annex D	Seismic Velocity Model Under Real-Life Situation With Buckle Folds
Annex E	Timetables At 9 Stations in Grid Size G = 0.2
Annex F	Objective Function Plot & Earthquake Location
Annex G	Cluster Of Earthquake Locations Under the Effect Of Random Error Within $\pm 0.2s$
Annex H	Density Distribution of Earthquake Under Random Errors

ANNEX A: Definition List

Term	Definition
P-waves	<p>Primary body seismic waves. P-waves are longitudinal, compressional waves that travel faster than other waves through the earth to arrive at seismograph stations (<i>receivers</i>) first, making them particularly useful for collection and analysis of seismic data.</p> <p>P-wave velocity depends on density and modulus of the medium it traverses, meaning the velocity of P-waves through a real-life medium will not be constant due to the inherent nature of the region's geology</p>
Receivers	Seismograph stations that record times of seismic occurrences
Grid	A discretised, specified spatial domain of computation
(Seismic) Velocity Model	Space of velocity values of P-waves in a grid
Origin time	Time of occurrence of an earthquake
Arrival Time	The first instance recorded of a P-wave for a given earthquake at a certain receiver
Receiver Time	Travel time of any grid point to a specified receiver
Timetable	Aggregate of receiver times of a receiver
Objective Function	Mathematical function of all the differences between the arrival time and receiver time (with the origin time considered) across all receivers

ANNEX B: Seismic Velocity Model

A grounded and realistic velocity model is crucially foundational in accurate earthquake relocations using the algorithms developed. As such, we utilise the well-studied model of the seismic structure in Transverse Ranges, California, as the basis for our velocity model. [4] provides a detailed description of this real-life model:

“Travel-time data obtained from both natural and artificial events occurring in southern California indicate a major, lateral crustal transition within the Transverse Range Province. The eastern crust is very similar to the adjacent Mojave region, where a crustal velocity of 6.2 km/sec is typically observed. The western ranges are dominated by an extensive 6.7 km/sec layer. P’s velocity beneath the western Mojave, Transverse Ranges, and northern Peninsular Ranges is 7.8 km/sec. The crustal thickness of these provinces is 30 to 35 km. The Transverse Ranges do not have a distinct crustal root. Unlike other provinces within southern California, the Transverse Ranges are underlain at a depth of 40 km by a refractor with a P-velocity of 8.3 km/sec. P-delays from a vertically incident, well-recorded teleseism suggest that this velocity anomaly extends to a depth of 100 km. [...] The regionally observed 7.8 km/sec layer is suggested as a zone of decoupling necessary to accommodate the horizontal shear that must result from the divergence of the crust and upper mantle plate boundaries. The geomorphic Transverse Ranges are viewed as crustal buckling caused by the enhanced coupling between the crust and upper mantle, which is suggested by the locally thin, 7.8 km/sec layer.”

Simulating the above P-wave velocities as they vary with depth yields the following model, as visualised in a simulated domain of depths (z-axis) up to 45 km over a distance (x-axis) of up to 150 km, we obtain the desired seismic velocity model.

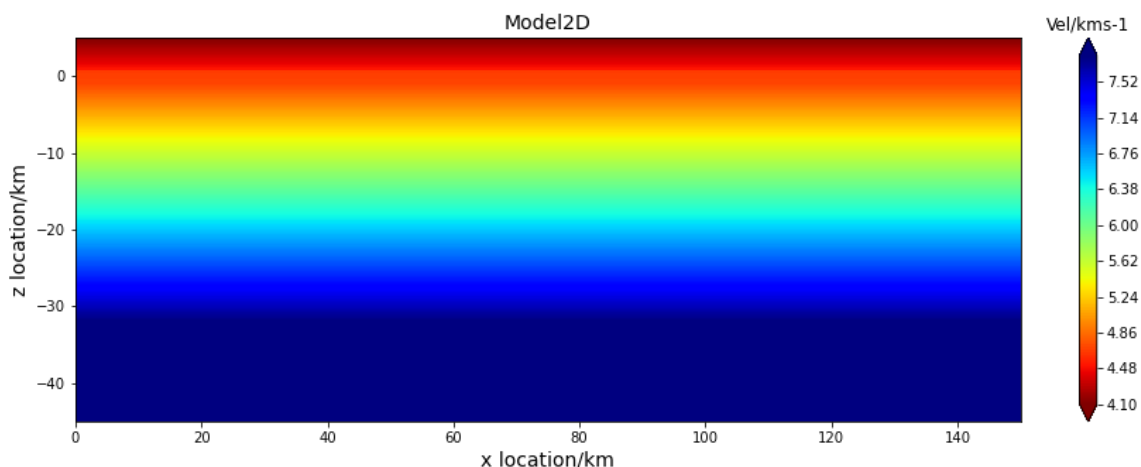


Fig 7. Map of real-life-inspired velocity model (named **Model2D**)

This same velocity model (**Model2D**) will be used throughout this report, even in different numerical tests of the algorithm.

ANNEX C: Solving Eikonal Equation By Fast Sweeping Method (Zhao, 2007)

To locate the earthquakes, the travel times of the earthquake to the receivers are required, as well as the timetables of each receiver in a common spatial domain. In this task where we have focused on the specifics of earthquake relocation, the generation of timetables was done by solving Eikonal equation: (2.1)

$$|\nabla u(x, z)|^2 = f(x, z)^2,$$

$$\text{i.e. } \nabla u(x, z) \cdot \nabla u(x, z) = \frac{1}{v(x, z)^2}, \quad x, z \in R$$

Where:

$f(x, z)$: slowness model,
 $v(x, z)$: velocity,

$u(x, z)$: travel time of P-wave from a reference point (e.g receiver) to (x, z)

with boundary condition:

$$u(x_k, z_k) = 0, \quad k \in \{1, 2, 3, \dots, 9\}.$$

(x_k, z_k) denoting coordinates of receiver k . This process can be expedited using a numerical method known as the Fast Sweeping Method (FSM) and its corresponding algorithm [7]. Henceforth, also define the grid size as h .

The Fast Sweeping Algorithm [7]

Discretization. Godunov upwind difference scheme [8] is used to divide the interior region, which excludes the boundary defined above, into discrete grid points:

(2.2)

$$[(u_{i,j}^h - \min(u_{i-1,j}^h, u_{i+1,j}^h))^+]^2 + [(u_{i,j}^h - \min(u_{i,j-1}^h, u_{i,j+1}^h))^+]^2 = f_{i,j}^2 h^2$$

$$i = 2, \dots, I - 1 \quad ; \quad j = 2, \dots, J - 1$$

Where:

$$(x)^+ = \begin{cases} x, & x > 0 \\ 0, & x \leq 0 \end{cases}$$

At the boundary of the computational domain, we use one-sided differences for discretisation.

Initialization. To enforce $u(x_k, z_k) = 0, k \in \{1, 2, 3, \dots, 9\}$, assign a fixed value of 0 at grid points (x_k, z_k) , which are at the receiver k . Assign variable, large positive values at all other grid points.

Gauss-Seidel iterations with alternating sweeping orderings. At each variable interior grid point we compute the solution \bar{u} to (2.2) from the current values of its neighbouring grid points and then update the value at the grid point to \bar{u} if it is lesser than it initially was; otherwise its value remains the same. We sweep the whole domain with four alternating orderings repeatedly:

$$(1) \ i = 1:I, j = 1:J, \quad (2) \ i = I:1, j = 1:J,$$

$$(3) \ i = I:1, j = J:1, \quad (4) \ i = 1:I, j = J:1.$$

To solve (2.2) for \bar{u} where $X = \min(u_{i-1,j}^h, u_{i+1,j}^h)$, $Y = \min(u_{i,j-1}^h, u_{i,j+1}^h)$:

$$(2.3) \quad \bar{u} = \begin{cases} \min(X, Y) + f_{i,j}h & |X - Y| \geq f_{i,j}h, \\ \frac{X+Y+\sqrt{2f_{i,j}^2h^2-(X-Y)^2}}{2} & |X - Y| < f_{i,j}h \end{cases}$$

One remark about the algorithm is that the large values in initialising interior grid points should be larger than the maximum possible value of $u(x, z)$ in the computational domain. This problem was avoided in our context as the real-life velocity of P-waves are widely known, finding an arbitrarily large value to be above which is trivial (e.g 100 km/s).

ANNEX D: Seismic Velocity Model Under Real-Life Situation With Buckle Folds

In reality, seismic stations do receive seismic data from earthquakes nearby. However, in reality, seismic data is often obtained in regions where the geology experiences buckle-folds in its strata [21]. To generally demonstrate the real seismic velocity model which differs slightly from region to region, we use **Model2D_true**.

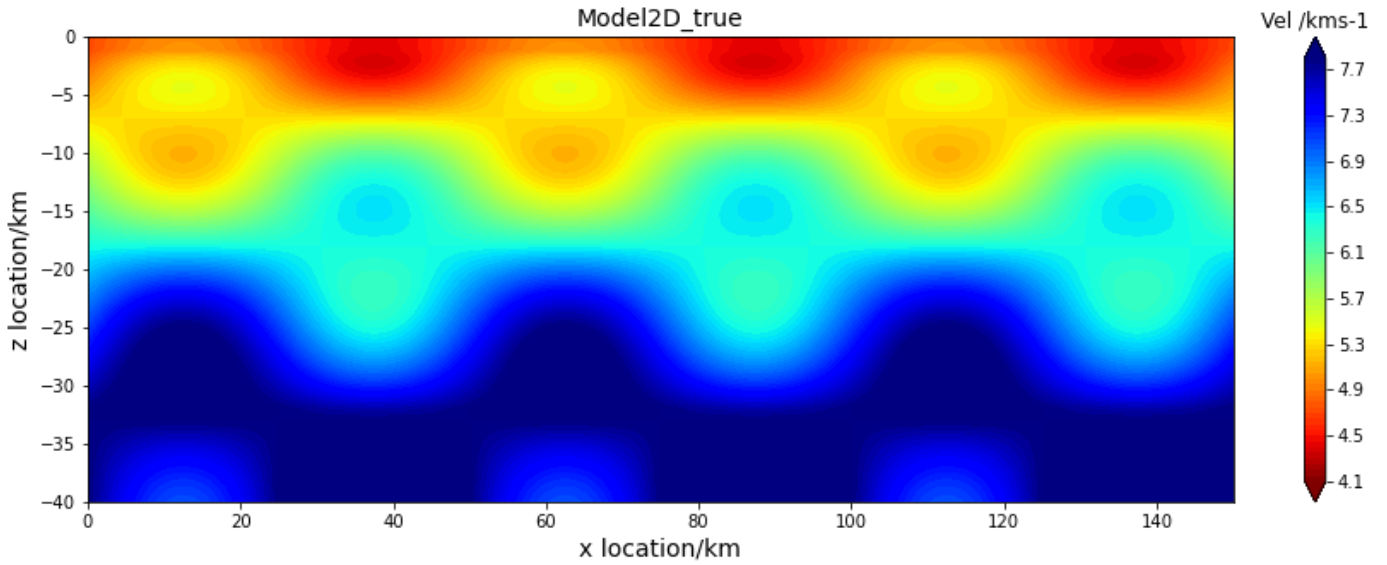


Fig 8. Velocity model from real-life seismic data under the influence of geological features (**Model2D_true**)

Note that the seismic velocity model in real life differs from one another due to the nature of geology, hence, the seismic velocity obtained in **Model2D** is not generalized enough to cater to real-life situations where geology plays an important role in deciding the actual seismic velocity model at that particular region. However, the generation of such real-life seismic data (any form of **Model2D_true**) can be executed to simulate the real-life situation with minimal inaccuracy.

Visually, the velocity yielded from the suggested modelling mathematical function above is largely similar to that of **Model2D_true** with errors of ± 0.64 km/s. This margin of error is considered small and acceptable as the relative error is low, of around less than 10%.

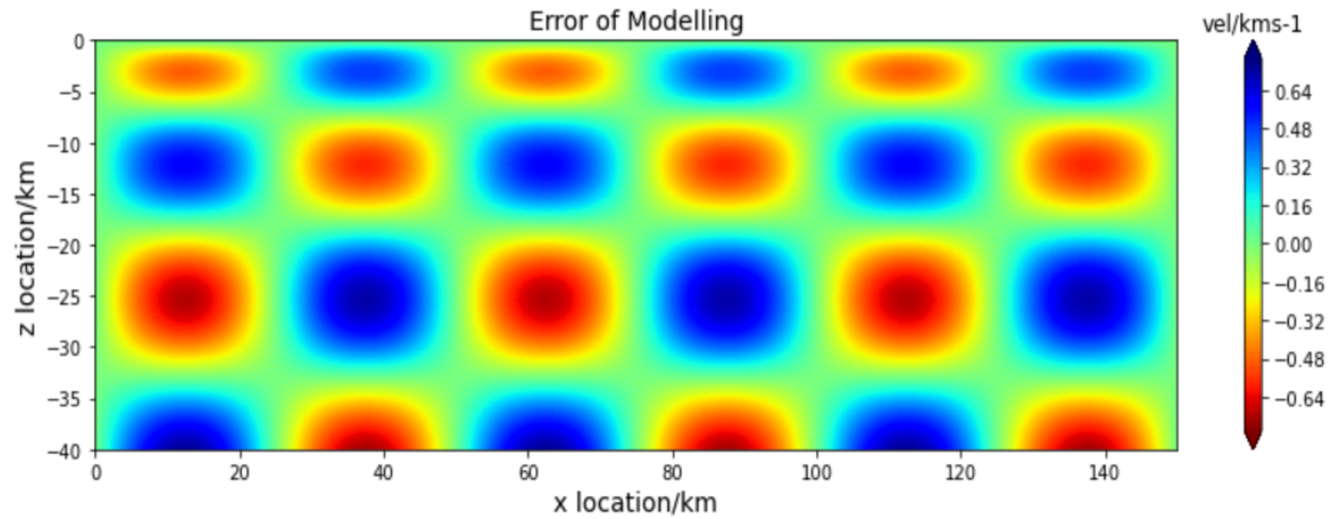
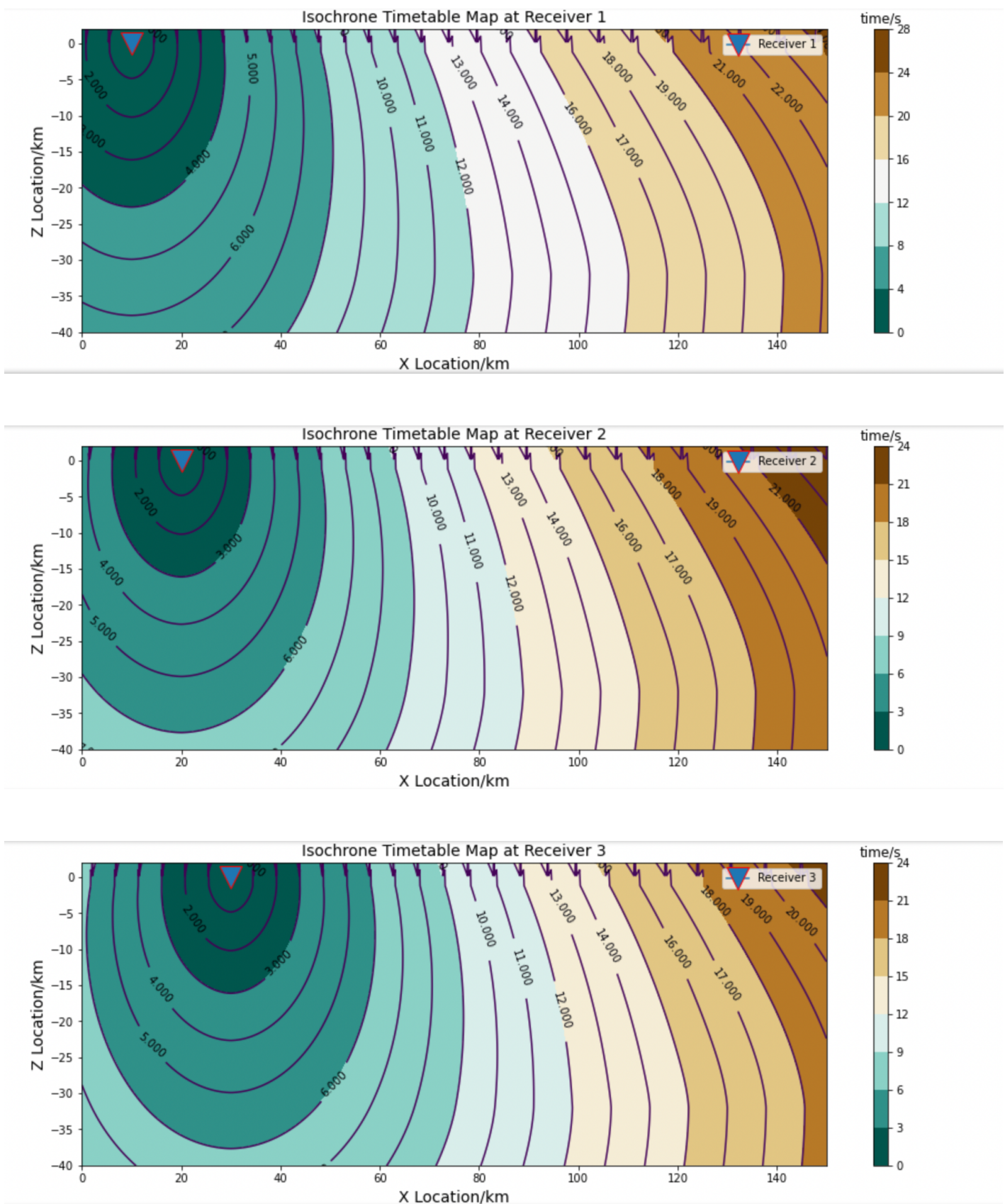
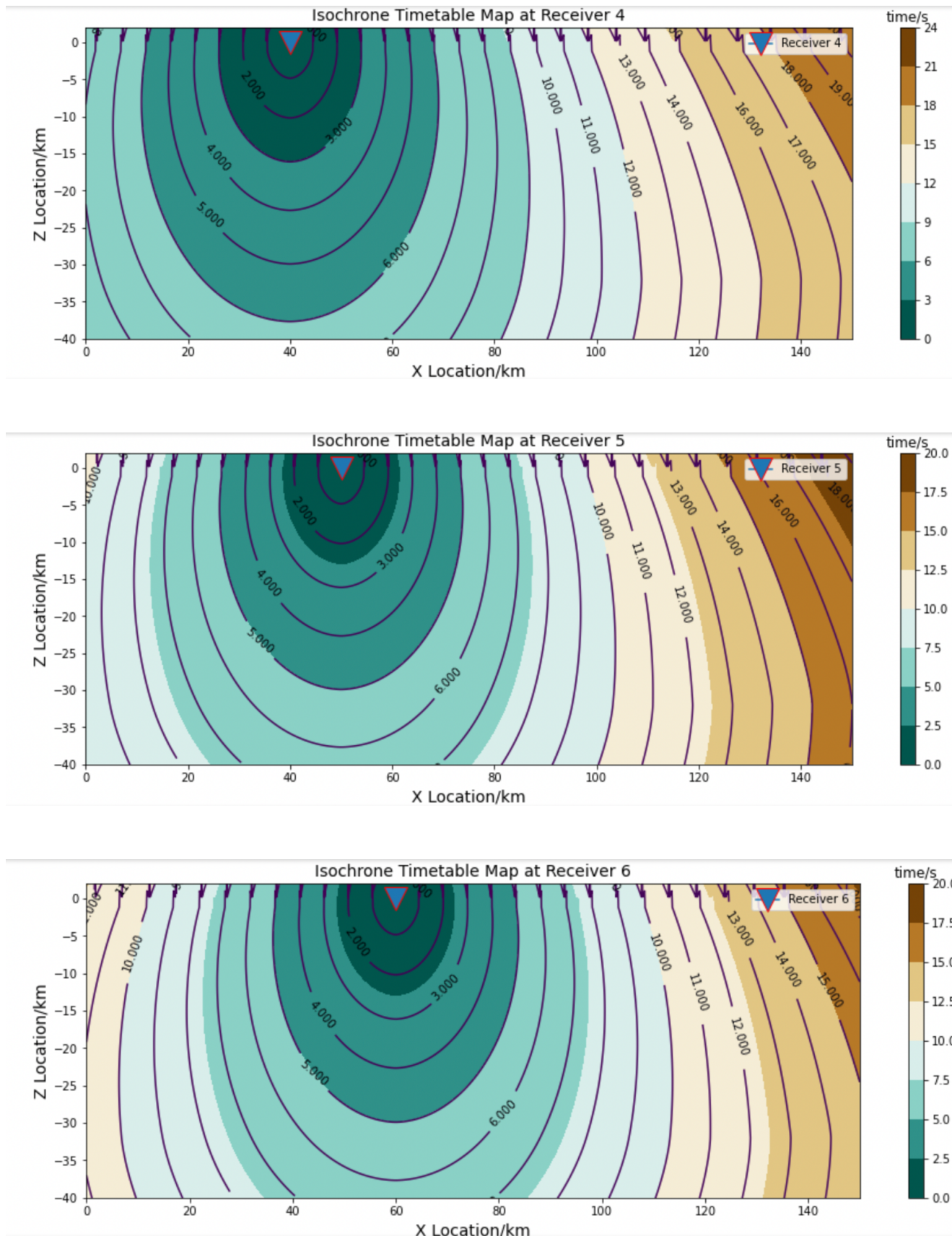


Fig 9. Insignificant error in re-modelling **Model2D_true**

ANNEX E: Timetables At 9 Stations In Grid Size $G = 0.2$





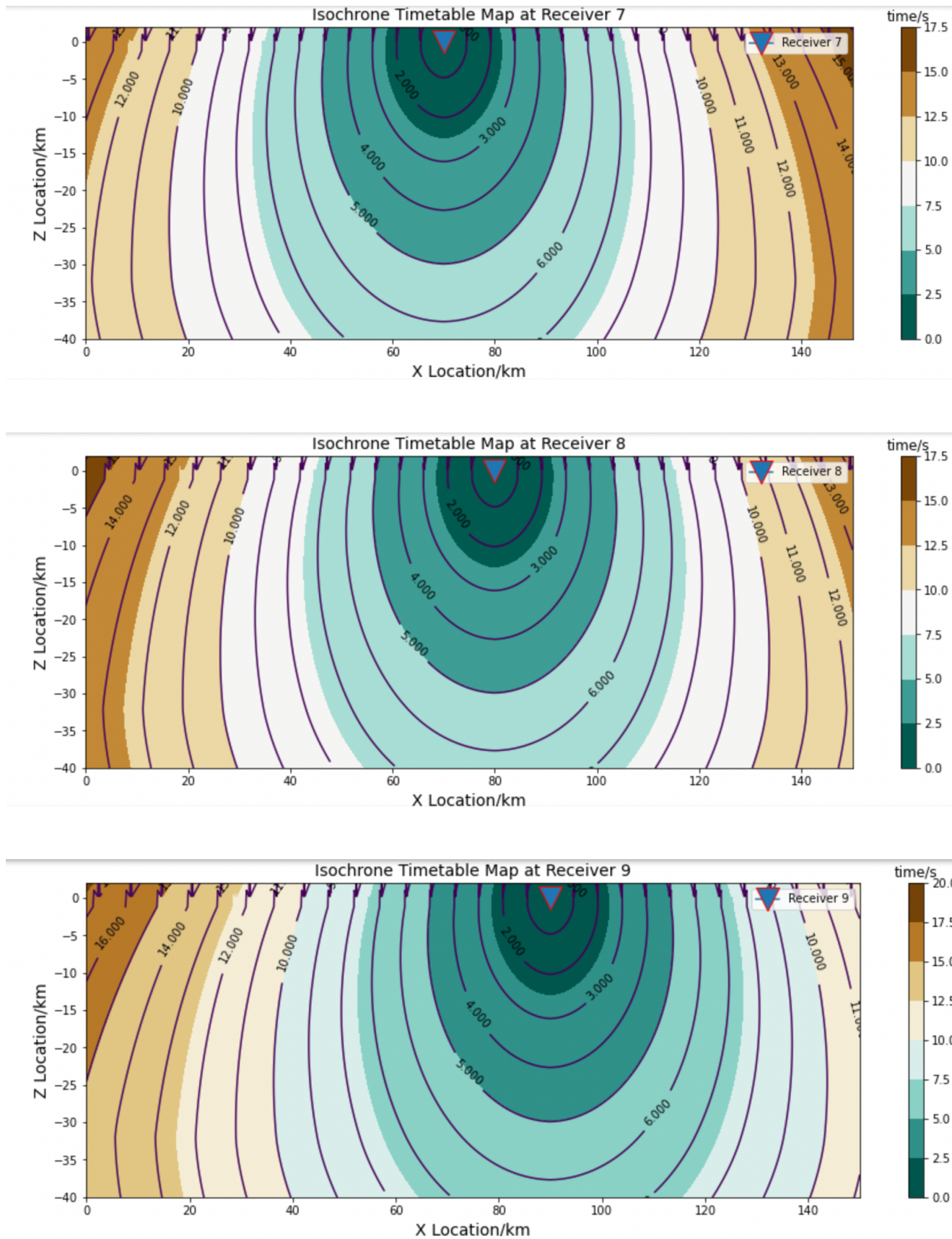


Fig 10. Example of Timetable from earthquake to 9 Receivers of $G=0.2$

ANNEX F: Objective Function Plot & Earthquake Location

The objective function varies with different grid points (i, j) yet achieves minimum value at grid point (i, j) where the earthquake is to be located. Isochrone map of Objective Function is plotted to demonstrate the possible locations where earthquake can be predicted to lie at and locations from where earthquake start will have the same value of objective function.

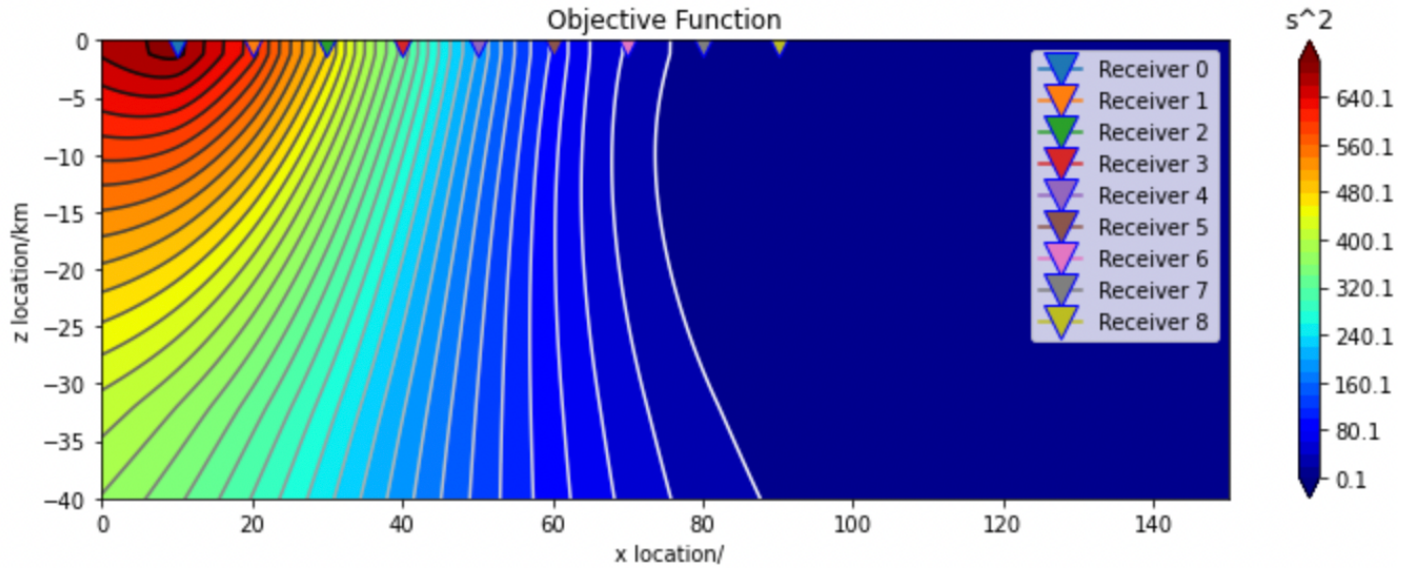


Fig 11. Values of Objective Function plotted on grid points

Similarly, the new located earthquake also achieves the minimum time difference from the real earthquake to grid points.

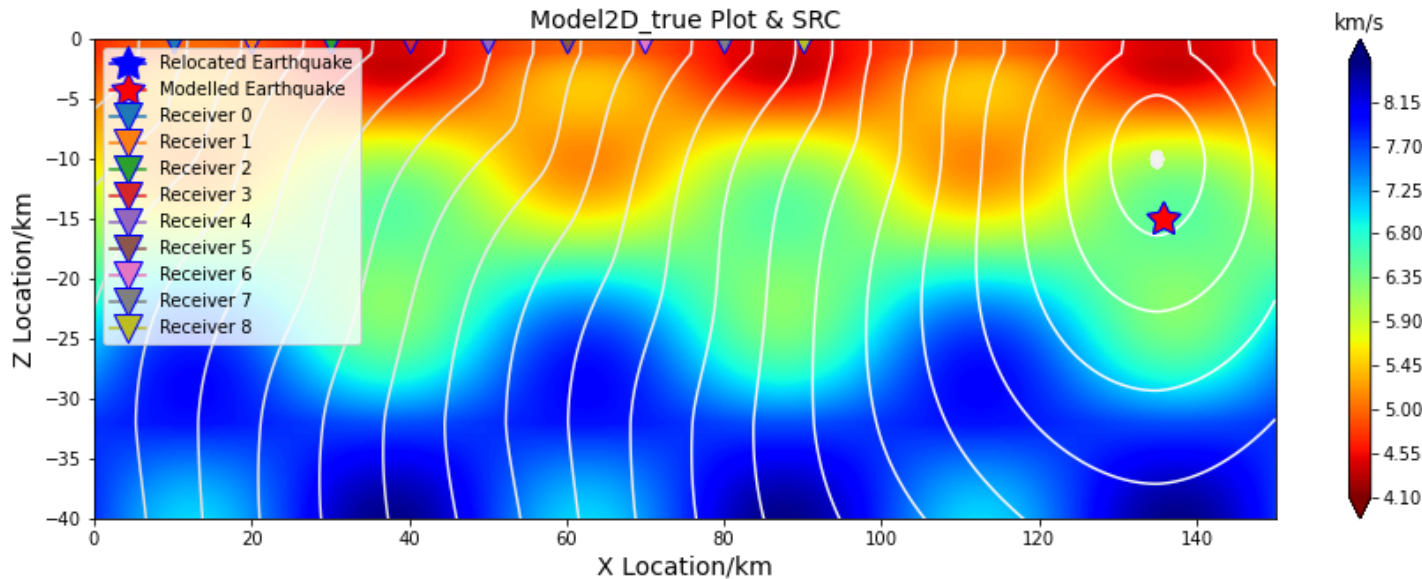
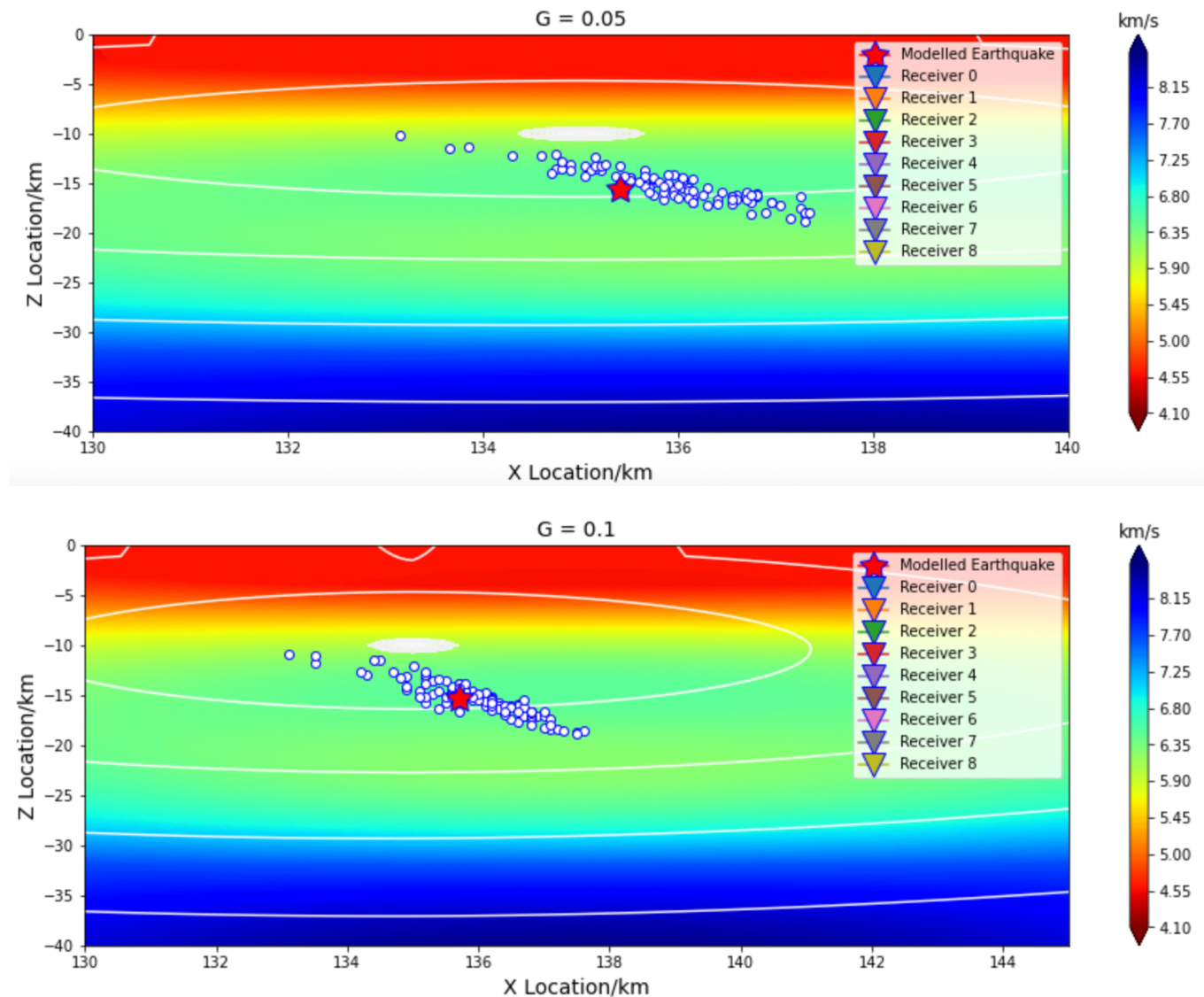


Fig 12. Matching time travel of relocated earthquake to grid points with that of modelled earthquake

ANNEX G: Cluster of Earthquake Locations Under The Effect Of Random Error Within $\pm 0.2s$

Uncertainties in earthquake locations are dominated by three factors [16], one of which is the measurement of errors of seismic arrival times [15]. To further study the accuracy of our Earthquake Location Model and its applicability and validity in real life, effects of those errors on the accuracy of earthquake location are studied. Sets of random errors ($N=100$) within a range of 0.2s to 0.2s [12] are generated at each station to simulate the situations in real life. 100 earthquake locations are found and observed to mainly cluster within a specific region despite few outliers observed in all 5 studied grid size models.



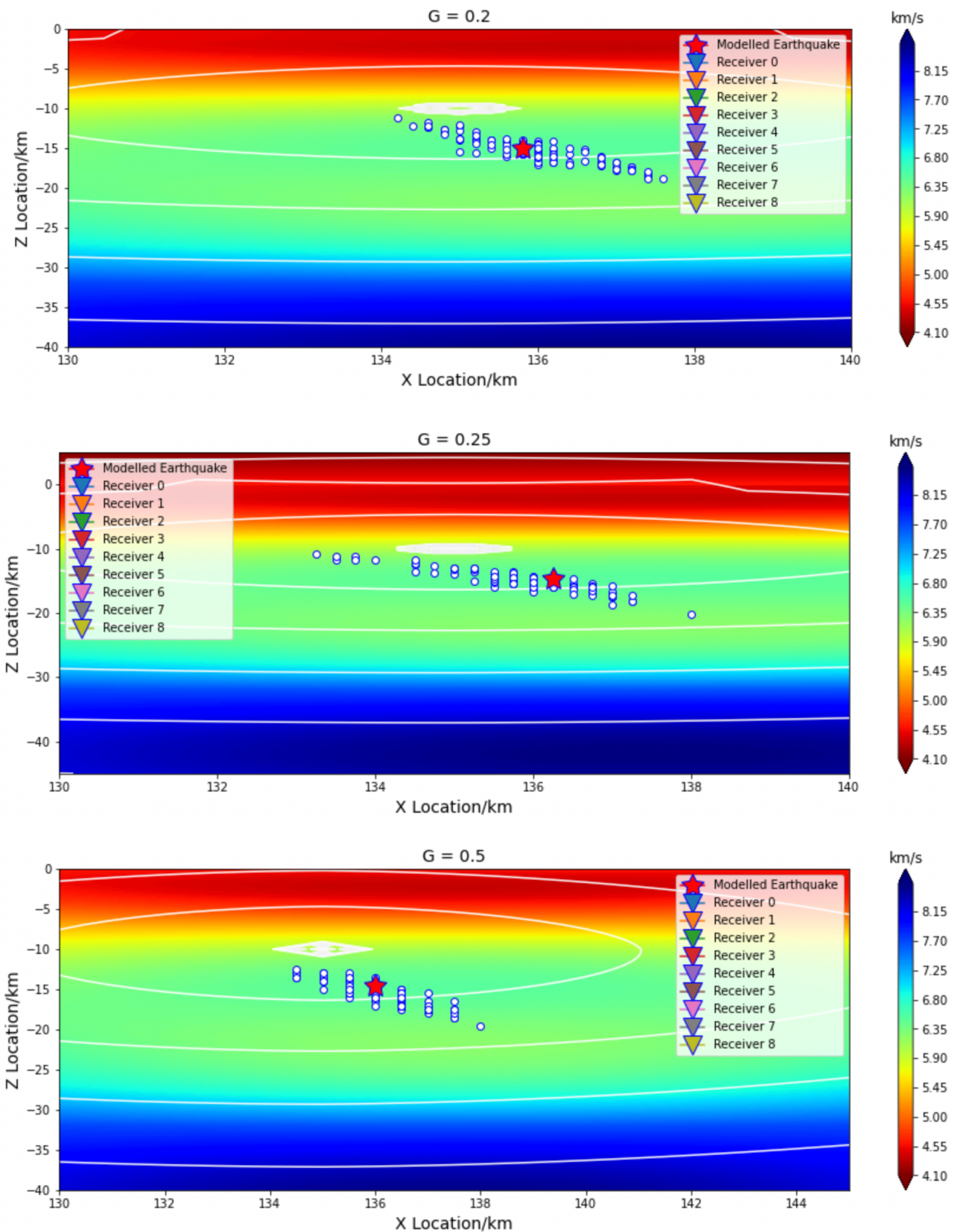


Fig 13. Cluster of earthquake locations under the random errors range of $\pm 0.2\text{s}$ seen with different grid sizes

ANNEX H: Density Distribution of Earthquake Under Random Errors

The investigation of how different sets of random errors influencing the arrival times at 9 stations assumes that each random error affects the earthquake location. Error of locating earthquake is measured as the distance between the modelled earthquake and the relocated earthquake. Multivariate linear regression model thus predicts the radius of region in which the relocated earthquake will lie in under the different sets of random errors. With sample of earthquake locations found with random errors ($N=100$), the predicted distance of the location of earthquake to the real earthquake is modelled. The density distribution is demonstrated by the density of overlap of circles demonstrating the predicted areas within which earthquake will lie.

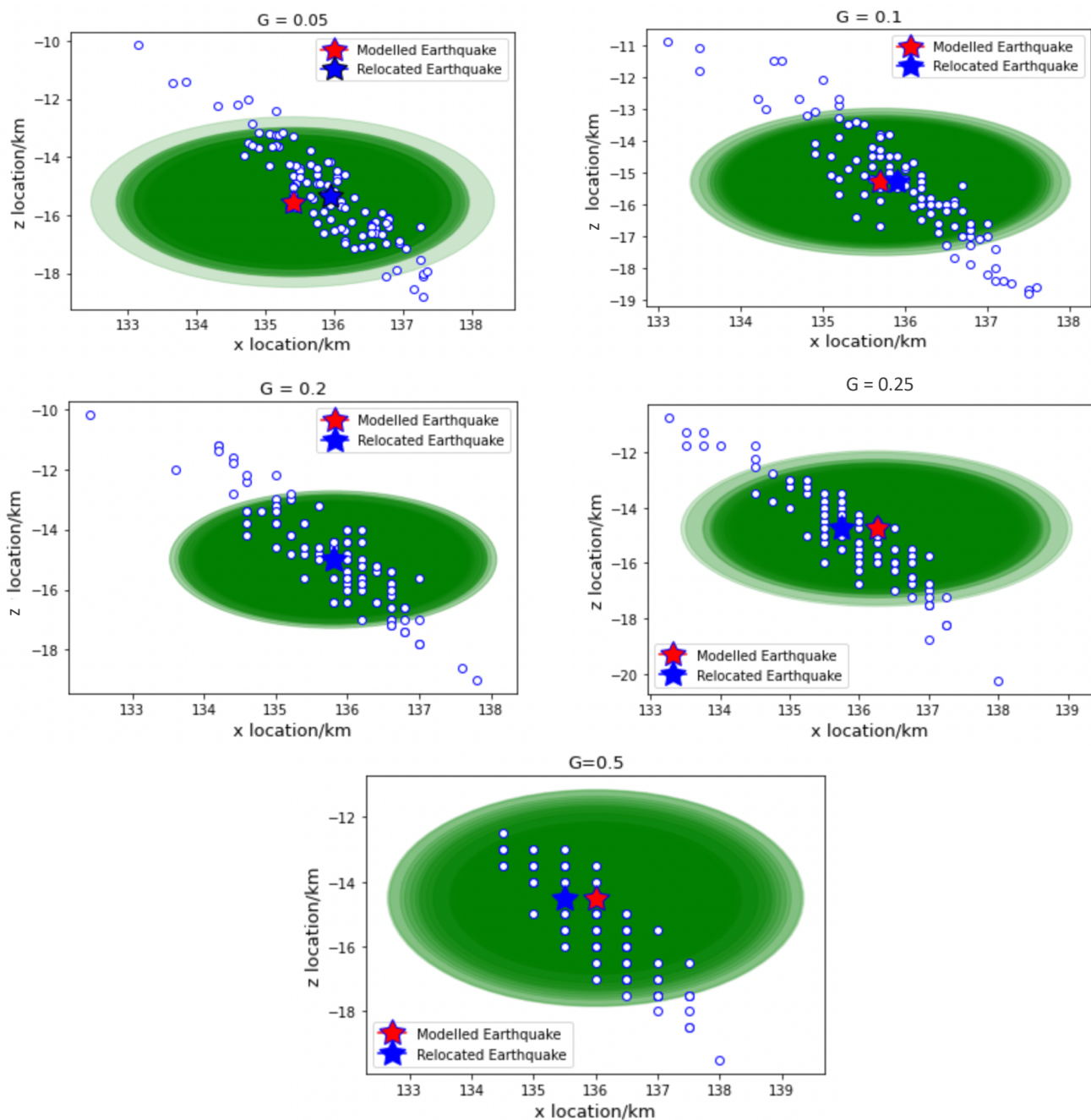


Fig 14. density distribution of earthquake location under the influence of random error of any range